Electrohydrodynamic surface microvortices for mixing and particle trapping

Leslie Y. Yeo[a)]
Micro/Nanophysics Research Laboratory Department of Mechanical Engineering, Monash University, Clayton, Victoria 3800, Australia

Diana Hou, Siddharth Maheshswari, and Hsueh-Chia Chang
Center for Microfluidics and Medical Diagnostics, Department of Chemical and Biomolecular Engineering, University of Notre Dame, Notre Dame, Indiana 46556

(Received 17 November 2005; accepted 1 May 2006; published online 8 June 2006)

We report a free-surface electrohydrodynamic flow phenomenon driven by an ionic wind mechanism induced by a high frequency gas-phase ac field (>10 kHz). Intense vortices >1 cm/s are generated above a critical voltage, beyond which the vortices break down to spawn off new vortex pairs leading to a cascade of vortices over a continuum of length scales; the mixing efficiency approaches a turbulent-like state. Colloidal particles are attracted and aggregated into planar crystal structures within the vortices by a combination of dielectrophoresis and shear-induced diffusion. © *2006 American Institute of Physics*. [DOI: 10.1063/1.2212275]

When a potential applied across a point and plate electrode above which a millimeter sized drop sample is placed [Fig. 1(a)] exceeds a threshold value for gas ionization, corona discharge occurs.[1] Plasma ions of similar polarity to the corona (point) electrode are then propelled away from the localized ionization region along the field lines in the direction of decreasing field intensity, consequently colliding with electroneutral air molecules. The transfer of momentum due to these collisions then result in a bulk electrohydrodynamic thrust towards the plate electrode known as *ionic wind*. Previous studies have shown that ionic propulsion directed towards a liquid interface can produce interfacial deformation[2] as well as internal liquid circulation.[3] The existence of ionic wind is demonstrated with smoke particles [Fig. 1(b)]; the air flow is absent when no field is applied.

Due to tangential shear at the air-liquid interface, intense surface vortices with linear velocities in excess of 1 cm/s are obtained. The mixing efficiency of the vortex flows is observed to approach that of turbulent mixing. In addition, colloidal particles present in the liquid are drawn into the vortices to form regimented crystals in the interior regions of the vortices. These particle aggregates are found to remain intact even after the removal of the electric field and the cessation of the flow, thus suggesting the potential of the device as an effective bioparticle trap. Both these phenomena have not been reported previously. The proposed microfluidic device is thus particularly suitable, albeit not limited, to microarray chips used in high throughput drug screening; the same micropipette or electrospray tip used to deliver the liquid sample onto the microarray can be used to induce the interfacial shear to drive the mixing or particle trapping.

The device consists of a liquid well, 8 mm in diameter and 3 mm deep, placed above a grounded plate [Fig. 1(a)]. An inclined sharp point electrode is brought into proximity (~4 mm) with the liquid and a high ac voltage is applied. When the point electrode is centered symmetrically, a vortex pair is produced. The various flow circulation patterns observed are shown in Fig. 1(c). Fluid motion only commenced above a critical voltage, ~1.9 kV if dc electric fields are employed. The critical voltage boundary, however, decreases with increasing frequency until a minimum ~0.4 kV (0 to peak) is attained at $f_c \sim 145$ kHz. Above f_c, the critical voltage boundary is observed to increase sharply again. A similar critical voltage minimum is also observed in the boundaries that delineate the transitions to other flow circulation patterns.

The observed minimum in the voltage-frequency characteristics at f_c is similar to that in a recently discovered ac electrospray phenomenon.[4] The correspondence is not surprising given the geometrical similarity (point and plate elec-

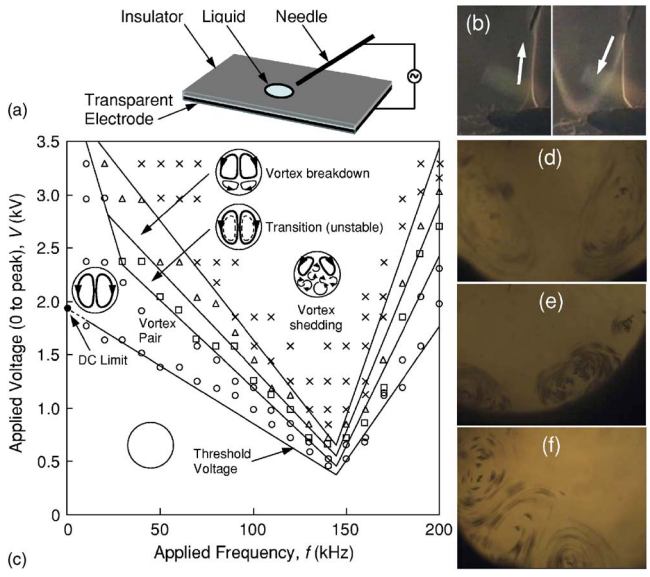

FIG. 1. (Color online) (a) Schematic illustration of the experiment. (b) Flow visualization with smoke particles; smoke particles rise by buoyancy from a source below the point electrode below the critical voltage (left panel) but are deflected downwards by the ionic wind beyond it (right panel). (c) Flow circulation behavior as a function of the applied voltage and frequency. (d) Dominant vortex pair at 2.9 kV (0 to peak) and 40 kHz. (e) Breakdown of the primary vortex at 3.3 kV (0 to peak) and 40 kHz to form a secondary vortex. (f) Vortex breakdown at 4.2 kV (0 to peak) and 50 kHz in which three secondary vortices are generated from the primary vortex.

[a)]Electronic mail: leslie.yeo@eng.monash.edu.au

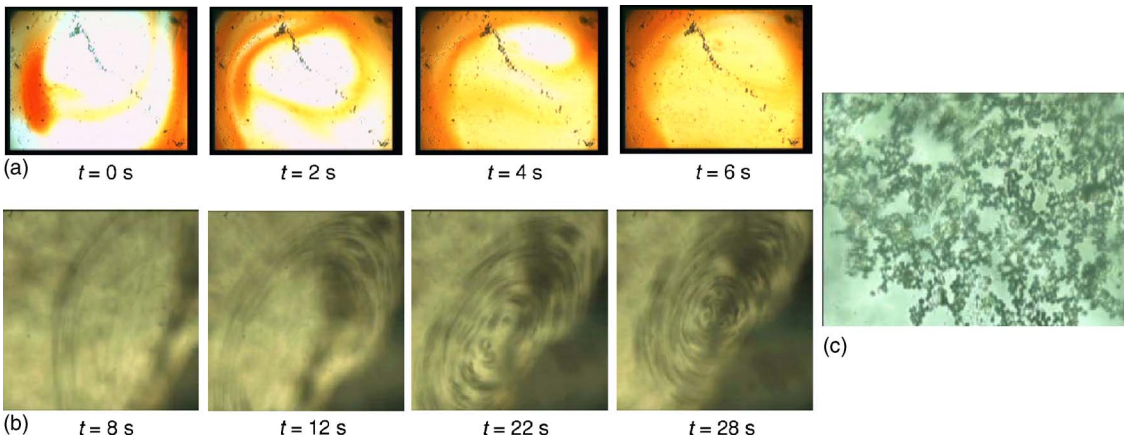

FIG. 2. (Color online) (a) Successive images in time t capturing the micromixing action of red food dye in water induced by electrokinetic interfacial shear. (b) Particulate aggregation in the vortex streamlines due to DEP force and shear-induced migration. (c) Particle aggregation is observed to remain intact after removal of the electric field and cessation of the flow.

trode configuration) and the high voltages involved. A similar plasma polarization mechanism[5] therefore is responsible for the observed voltage-frequency minimum. Due to differing positive and negative plasma mobilities, a negative plasma cloud persists around the point electrode. In the anodic half cycle, the external field is effectively screened and there is no net Coulombic force that causes ion drift away from the point electrode. In the cathodic half cycle, however, when the point electrode and the surrounding plasma possess opposite polarities, the field is effectively enhanced and a net Coulombic force exists to drive plasma electromigration and hence the electrohydrodynamic thrust. At low frequencies, the plasma cloud has sufficient time to diffuse away, thus lowering the field enhancement effect of the plasma cloud. As such, higher critical voltages are required. At high frequencies, there is insufficient time for plasma generation and again plasma field enhancement diminishes. The optimum frequency f_c corresponding to the voltage minimum therefore exists and can be related to the inverse $\mathcal{RC}$ time scale of the plasma charging mechanism, where $\mathcal{R}$ is the resistance across the electrodes and $\mathcal{C}$ is the plasma double layer capacitance. From our measurements, $\mathcal{R}\sim 20$ MΩ and $\mathcal{C}\sim 0.3$ pF, giving $1/\mathcal{RC}\sim 160-170$ kHz, close to f_c.

The primary interfacial vortex pair [Fig. 1(d)] becomes unstable with increasing applied voltages and frequencies and eventually breaks down to spawn off an additional vortex pair, as shown in Figs. 1(e) and 1(f), the primary vortex pair itself shrinking considerably in size. Subsequent increases in the voltage and frequency quickly lead to further vortex breakdown such that a turbulent-like state involving a cascade of vortex structures over a continuum of length scales is almost immediately approached, similar to that in vortex shedding; this vortex cascade is responsible for turbulent-like mixing efficiencies. With further increases in the applied frequency while maintaining a constant voltage, however, the stability of the vortices is recovered, as noted by the transition into the right arm of the V-shaped window in Fig. 1(c).

The potential of the device as an effective micromixer is shown in Fig. 2(a). Without agitation, the diffusion of the dye requires over 20 min. Upon application of the field, the diffusion limitation is removed through the introduction of the interfacial vortex flow with characteristic Péclet number $\mathrm{Pe}\equiv\langle u_l\rangle\mathcal{L}/\mathcal{D}$ above 10^3, where $\langle u_l\rangle$ is the convective velocity, $\mathcal{L}\sim 10^{-3}$ m is the characteristic length scale, and $\mathcal{D}$ is the diffusivity. We observe the fluid to be well mixed in $\sim$6 s; optimization of the system parameters to increase Pe by increasing $\langle u_l\rangle$ or by increasing turbulence such that the effective diffusivity is reduced lowers the mixing time by an order of magnitude. In fact, the vortex mixing efficiency approaches that of turbulent-like mixing at higher voltages and frequencies with the breakdown of vortices into structures with a continuum of length scales.

In contrast to solutes, which are dispersed by the vortices, colloidal particles consisting of 10 μm polystyrene particles suspended in the liquid are observed to aggregate within the vortices to form planar interfacial colloidal crystals, as shown in Fig. 2(b). At frequencies below 100 kHz, it has been shown that positive dielectrophoresis (DEP) of polystyrene particles occurs (they move towards the high-field region), despite the prediction of the classical Maxwell-Wagner theory.[6,7] This crossover to positive DEP is sometimes explained by correcting the classical theory with a new relaxation time involving a conducting Stern layer.[8] We hence attribute the convergence of the particles into a ring to be due to their positive DEP motion towards a point on the interface that is closest to the needle and hence has the highest field. As this point is part of a closed streamline within the interfacial vortex and as the convection velocity is higher than the DEP velocity or the shear-induced migration velocity towards the vortex center, the particle distribution is quickly homogenized within the closed streamline to form a ring structure. Cross-streamline transport then ensues due to shear-induced particle interaction and results in particle population of the vortex interior. This is evident in the reduction of the vortex velocity with increasing particle concentration in the vortex. This final packing at the vortex center then causes the formation of large particle aggregates due to van der Waals forces, although some aggregation can begin within the ring structure.

Particle aggregation into regimented crystals only occurs within the vortex where the particle concentration is higher and where hydrodynamic shear is lower. In parallel flow, the shear rate is known to promote particle interaction across streamlines with an interaction rate of $\phi\dot{\gamma}$, where ϕ is the local particle volume fraction in the vortex, measured by employing a pixel intensity analysis on the acquired images,

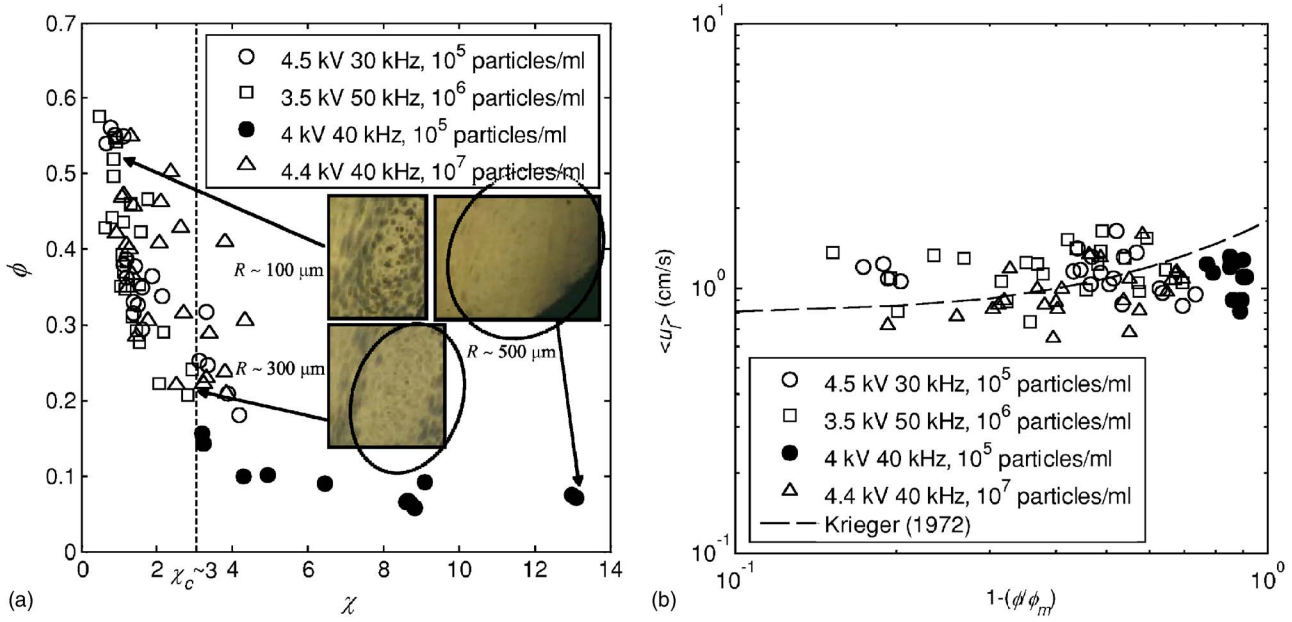

FIG. 3. (Color online) (a) Change in instantaneous vortex particle volume fraction ϕ with the ratio between the DEP and shear-induced migration velocities χ for a suspension of 10 μm polystyrene particles in DI water. The open data points represent events concentrated particles are on the periphery forming a concentrated ring, whereas the solid data points represent events in which particle invasion into the vortex interior occurred. (b) Particle convective velocity $\langle u_l \rangle$ as a function of ϕ for a suspension of 10 μm polystyrene particles in DI water, indicating good agreement with the correlation of Ref. 10.

and $\dot{\gamma}$ is the shear rate within the vortex, observed to exceed 100 s^{-1}. With a scatter length comparable to the particle size a, such multiparticle interaction produces an effective cross-streamline particle diffusion rate of $\dot{\gamma}\phi a^2$.[9] When ϕ within the periphery annulus exceeds a critical value, dispersion into the high-shear-rate vortex becomes significant, as seen in Fig. 2(b). The diffusion time into a vortex of radius R is $(R/a)^2/(\gamma\phi)$ and is estimated to be $\sim 10^4$ s based on a bulk value for ϕ of 0.01 but reduces to 1–10 s when ϕ reaches the hard sphere maximum packing $\phi_m = 0.68$, the latter consistent with the time lapse in the frames of Fig. 2(b). The maximum packing at the periphery and eventually at the vortex interior causes the particle contact and forms planar aggregate structures held together by van der Waals forces which remain intact even after termination of the electric field and interfacial flow [Fig. 2(c)] unless vigorously stirred.

Figure 3(a), which plots ϕ against the ratio between the characteristic DEP velocity, $U_{\mathrm{DEP}} \sim \epsilon \nabla |E|^2 a^2/\mu$, and the shear-induced migration velocity of a particle in the vortex, $U \sim \dot{\gamma} a^2 \phi / R \sim$, i.e., $\chi \sim U_{\mathrm{DEP}}/U$, shows the competition between the two mechanisms. ϵ is the liquid permittivity, E is the field, and μ is the viscosity; note that χ is independent of a. Instantaneous values of ϕ and χ were measured as the vortex evolved in time for different shear rates, applied fields, and particle radii. A critical value $\chi_c \sim 3$ is observed below which shear-induced migration dominates resulting in population of the vortex interior. R also decreases with diminishing χ until χ_c is reached. The vortex size then remains constant and ϕ begins to increase. The reduction in $\langle u_l \rangle$ with increasing ϕ and hence the effective suspension viscosity μ_r are also observed in Fig. 3(b) and are shown to agree well with the empirical correlation in Ref. 10 where $\mu_r = (1 - \phi/\phi_m)^{-1.82}$.

[1] L. B. Loeb, *Electrical Corona* (University of California Press, Berkeley, 1965).
[2] H. Kawamoto and S. Umezu, J. Phys. D **38**, 887 (2005).
[3] R.-I. Ohyama, K. Kaneko, and J.-S. Chang, IEEE Trans. Dielectr. Electr. Insul. **10**, 57 (2003).
[4] L. Y. Yeo, D. Lastochkin, S.-C. Wang, and H.-C. Chang, Phys. Rev. Lett. **92**, 133902 (2004).
[5] S. Maheshwari, L. Y. Yeo, and H.-C. Chang (unpublished).
[6] L. Gorre-Talini, S. Jeanjean, and P. Silberzan, Phys. Rev. E **56**, 2025 (1997).
[7] H. Morgan and N. G. Green, *AC Electrokinetics: Colloids and Nanoparticles* (Research Studies, Baldock, Hertfordshire, 2003).
[8] Z. Gagnon and H.-C. Chang, Electrophoresis **26**, 3725 (2005).
[9] D. Leighton and A. Acrivos, J. Fluid Mech. **181**, 415 (1987).
[10] I. M. Krieger, Adv. Colloid Interface Sci. **3**, 111 (1972).